



Precise control of selective hydrogenation of α,β -unsaturated aldehydes in water mediated by ammonia borane

Yangyang Zhou^{a,*}, Chen Chen^a, Qiling Li^a, Yanbo Liu^a, Ting Wei^a, Youzhen Liu^a,
Zebing Zeng^{a,*}, Darren Bradshaw^b, Bing Zhang^{a,c}, Jia Huo^{a,c,**}

^a Advanced Catalytic Engineering Research Center of the Ministry of Education, Provincial Hunan Key Laboratory for Graphene Materials and Devices, State Key Laboratory of Chemo/Biosensing and Chemometrics, College of Chemistry and Chemical Engineering, Hunan University, Changsha, Hunan 410082, PR China

^b School of Chemistry, University of Southampton, Highfield, Southampton SO17 1BJ, UK

^c Hunan Provincial Key Laboratory of Advanced Materials for New Energy Storage and Conversion, Hunan University of Science and Technology, Xiangtan 411201, PR China

ARTICLE INFO

Keywords:

α -unsaturated aldehydes
Hydrogenation selectivity
Ammonia borane
Metal organic layer
Pd based catalyst

ABSTRACT

Hydrogenation of unsaturated biomass in a control manner is highly desirable but challenging, especially under mild conditions. We here report selective hydrogenation of α,β -unsaturated aldehydes (UALs), featuring a precise control of all potential products by adjustment of the role of ammonia borane (AB) in transfer and/or catalytic hydrogenation. The hydrogenation can be readily operated in neat water without using any external H_2 -source, because AB as the H_2 -source is favorable in aqueous solution. Impressively, unsaturated alcohols are prepared in 100% conversion by the room-temperature transfer hydrogenation of UALs with AB, while saturated aldehydes are obtained in 100% conversion and > 90% selectivity with high activity (i.e., turnover frequency = 0.98 s^{-1} for cinnamaldehyde), by the catalytic hydrogenation with H_2 released from AB and Pd immobilized on two-dimensional metal organic layer. On the other hand, UALs can be completely converted into the saturated alcohols through a combination of transfer and catalytic hydrogenation in one pot. This strategy can be extended to more than 8 types of UALs, and provides a facile way to fine-control the selective hydrogenation of unsaturated compounds with competing bonds.

1. Introduction

Biomass conversion represents a sustainable strategy to meet the increased demand for renewable resources and alleviate the environmental pollution [1–4]. As one of the key biomass conversion processes, hydrogenation of α,β -unsaturated aldehydes (UALs) has provided substantial feedstocks for the fine chemical industry [5–8]. For example, hydrogenated products of cinnamaldehyde (CAL), including cinnamyl alcohol (COL), hydrocinnamaldehyde (HCAL) and phenyl propanol (HCOL) are very important intermediates in fields of perfumes, flavors, and pharmaceuticals (Scheme 1) [9–12]. It is worth noting that their effect/function will vary from product to product, which necessitates the precise control of hydrogenation as demanded. However, the presence of multiple competing unsaturated bonds makes it difficult to

achieve this ultimate goal [11]. Furthermore, the hydrogenation of UALs was often performed with high-pressure H_2 and in organic solvents, which is incompatible with the requirement of sustainability [5–7]. Therefore, it is highly desirable but challenging to develop a hydrogenation strategy to precisely control the hydrogenation selectivity under environmentally benign conditions [13,14].

Selective hydrogenation of UALs is mainly challenged by the presence of two unsaturated bonds ($C=O$ and $C=C$), especially the unflavored thermodynamics of $C=O$ hydrogenation [9,12,15]. Various strategies have been employed for improving the hydrogenation selectivity of $C=O$ or $C=C$ [16–25], especially the combination of metal organic frameworks (MOFs) and metal nanoparticles [26–29]. Tang and co-workers [12,30] designed a sandwiching structure, where Pt nanoparticles were confined between core and shell composed of the same

* Corresponding author.

** Corresponding author at: Advanced Catalytic Engineering Research Center of the Ministry of Education, Provincial Hunan Key Laboratory for Graphene Materials and Devices, State Key Laboratory of Chemo/Biosensing and Chemometrics, College of Chemistry and Chemical Engineering, Hunan University, Changsha, Hunan 410082, PR China

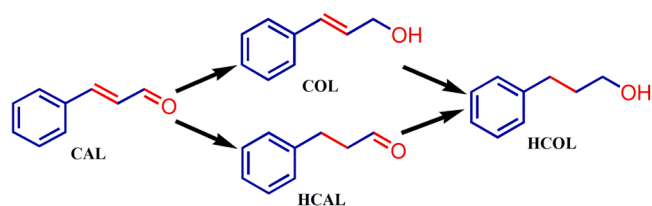
E-mail addresses: zbzeng@hnu.edu.cn (Z. Zeng), jiahuo@hnu.edu.cn (J. Huo).

<https://doi.org/10.1016/j.apcatb.2022.121348>

Received 15 February 2022; Received in revised form 22 March 2022; Accepted 23 March 2022

Available online 29 March 2022

0926-3373/© 2022 Elsevier B.V. All rights reserved.



Scheme 1. Three potential products for CAL hydrogenation.

MOF, MIL-101. Strong interaction between C=O and unsaturated metal sites of MIL-101 has resulted in excellent CAL conversion of 94.3% and COL selectivity of 97%. Huo et al. have successfully increased the unsaturated alcohol selectivity by controlling the steric hindrance around Pt nanoparticles through wrapping with different MOFs [31]. Liu et al. [32] deposited Pt nanoparticles on an acidic MOF for CAL hydrogenation to HCAL with > 99.9% selectivity and conversion because of the screening effect of C=O in CAL with Lewis acid sites in the MOF. Although enormous efforts have been invested on increasing the hydrogenation selectivity of C=O or C=C, respectively, it is still not achievable to precisely control the selective hydrogenation of UALs for all potential products over a reagent.

Herein, we report an ammonia borane (AB)-mediated approach to precisely control the selective hydrogenation of UALs towards all potential products by simply switching the roles of AB in transfer and/or catalytic hydrogenation. The hydrogenation was readily operated in neat water without using any external H₂-source. AB is a stable, nontoxic and recyclable solid hydrogen storage material with high hydrogen content (ca. 19.6 wt%) and high solubility in water. AB can serve as not only a reductant for transfer hydrogenation, but also a safe hydrogen source for catalytic hydrogenation [33–39]. Berke et al. [33] have demonstrated that polarized unsaturated bonds (polar olefins, aldehydes, ketones, and imine) could be stoichiometrically hydrogenated by AB through a double-H transfer mechanism. Since UALs contains polarized (C=O) and unpolarized (C=C) unsaturated bonds, AB is

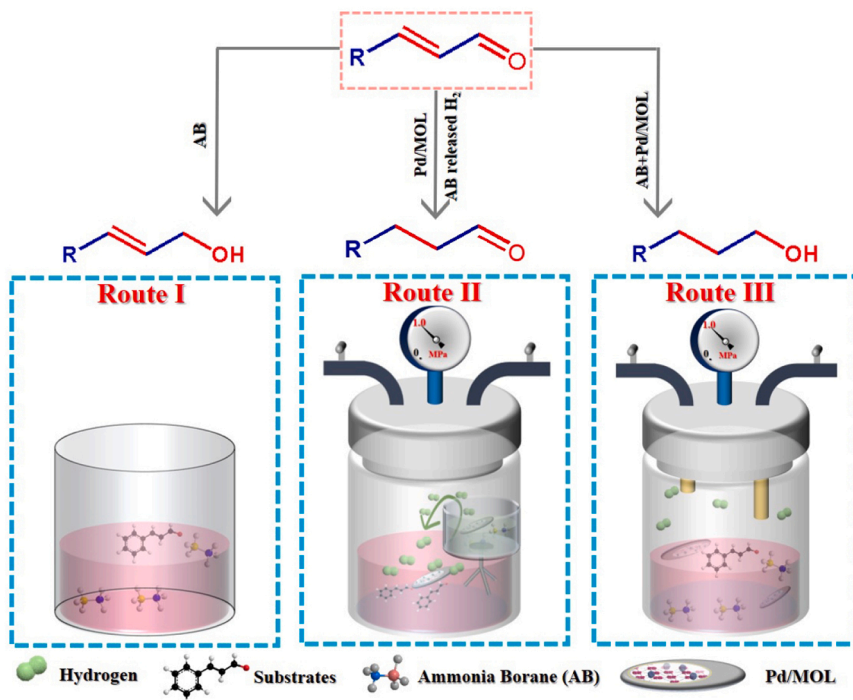
expected to selectively reduce C=O instead of C=C to produce unsaturated alcohols (UOLs) through the transfer hydrogenation (**Route I** in **Scheme 2**). The exclusive hydrogenation of C=O by AB has been confirmed in the organic solvents in our previous work [37]. Because of the excellent water solubility of AB, it is envisaged that AB could exclusively produce UOLs in water as well. Besides, saturated aldehydes (SALs) could be prepared by employing AB as the hydrogen source and through catalytic hydrogenation with a catalyst for selective reduction of C=C bonds (**Route II** in **Scheme 2**). Finally, UALs could be completely hydrogenated into saturated alcohols (SOLs) by taking full advantage of AB as both H-transfer agent and H₂-source (**Route III** in **Scheme 2**). Therefore, all potential hydrogenated products would be prepared through the dynamic combination of the transfer and catalytic hydrogenation mediated by AB under mild conditions.

In this work, this strategy is successfully achieved by employing AB for both exclusive transfer hydrogenation and safe hydrogen storage, and a Pd based catalyst for both dehydrogenation of AB and catalytic hydrogenation of C=C double bonds. Exclusive hydrogenation of UALs into UOLs is easily realized by room-temperature transfer hydrogenation of UALs by AB. Pd immobilized on a two-dimensional metal organic layer (Pd/MOL) was chosen for dehydrogenation of AB to produce H₂ and catalytic conversion of UALs into SALs with > 90% of conversion and > 90% of selectivity. Besides, full hydrogenation of UALs is achieved by using AB and Pd/MOL together in the neat water, where AB serves as both the transfer hydrogenation agent and H₂-source, and Pd/MOL simultaneously dehydrogenate AB and catalytically hydrogenate C=C bonds with released H₂. Hence, all three hydrogenated products are precisely controlled in environmentally benign solvents without using any external high pressure H₂-source.

2. Experimental section

2.1. Chemicals and reagents

Chemical reagents, such as, 2,2'-bipyridine-5,5'-dicarboxylic acid (H₂BPYDC), zirconium tetrachloride (ZrCl₄), palladium dichloride



Scheme 2. Proposed routes for precise control of selective hydrogenation of UALs mediated by AB. **Route I:** conversion of UALs into UOLs with AB in an open autoclave; **Route II:** conversion of UALs into SALs in an autoclave with inner lining for hydrogen production from AB decomposition by Pd/MOL and outer lining for hydrogenation of UALs catalyzed by Pd/MOL; **Route III:** complete hydrogenation of UALs with AB and Pd/MOL to SOLs in a closed autoclave.

(PdCl₂), Pd/C (10% loading), sodium borohydride (NaBH₄), formic acid (HCOOH), N,N-dimethylformamide (DMF), n-dodecane, tetrahydrofuran (THF), ethanol, ammonia borane (NH₃·BH₃), polytetrafluoroethylene (PTFE) preparation (60 wt%), cinnamaldehyde, cinnamyl alcohol, hydrocinnamaldehyde, phenylpropanol, (E)-3-(p-tolyl)acrylaldehyde, 4-fluorocinnamaldehyde, trans-4-bromo-cinnamaldehyde, 4-methoxycinnamaldehyde, acrolein, trans-2-pentenal, 2-methyl-2-butenal were purchased from Energy Chemical, Aladdin, Innochem companies. Deionized water was purified in the lab with a specific resistance of 18.25 MΩ·cm. All chemical reagents in this work were commercially purchased and used without further purification.

2.2. Preparation of catalysts

2.2.1. Preparation of the MOL

MOL was synthesized according to the published literature [40]. Synthesis of MOL was performed in a 5 mL glass vial with Teflon caps. ZrCl₄ (5 mg, 21.5 μmol) and H₂BPYDC (5 mg, 20.5 μmol) were dispersed in the mixture solution of DMF (1 mL), water (1 mL) and HCOOH (0.16 mL). Then, the vial was sonicated for 30 min until the solution became clear, which was transferred to an oven at 120 °C for 48 h. After gradually cooling to room temperature, pale white suspension was centrifuged and suspended in DMF (5 mL) at 60 °C for 6 h to remove unreacted substrates. The obtained solid was further washed with DMF and THF for three times, and ca. 5 mg sample was obtained for further use after 150 °C vacuum drying.

2.2.2. Preparation of Pd/MOL

Firstly, the pre-activated MOL sample (10 mg) was added into 3 mL water, and sonicated for 15 min until the mixture dispersed well. Then, as-prepared 50 μL K₂PdCl₆ solution (10 mg mL⁻¹) was dropwise added to the above suspension under vigorous stirring. After stirring for 24 h at room temperature, the Pd⁴⁺/MOL was washed by 5 mL deionized water for three times to remove the unabsorbed Pd⁴⁺ and dried in vacuum (yield ca. 10 mg). Reduction processes: 10 mg Pd⁴⁺/MOL was dispersed in 3 mL water, and 8 mg NaBH₄ in 1 mL water was dropwise added into the mixture containing Pd⁴⁺/MOL, which was stirred for 3 h at room temperature. After washed by 5 mL deionized water for three times, Pd/MOL was obtained and dried in vacuum (yield ca. 10 mg).

2.2.3. Preparation of UiO-67-bpy

UiO-67-bpy was synthesized according to the literature procedure [41,42]. ZrCl₄ (24.5 mg, 0.106 mmol) and H₂BPYDC (26 mg, 0.104 mmol) were dispersed in the mixture solution of HCOOH (1 mL) and DMF (10 mL) in a 20 mL glass vial under sonication for 30 min until the solution became clear, which was transferred into and keep 120 °C for 24 h. The resulted solid was washed with DMF and THF for 3 times, dried at 60 °C and activated at 150 °C for further use. (12 mg, 60% yield).

2.2.4. Preparation of Pd/UiO-67-bpy

The procedure of Pd⁴⁺/UiO-67-bpy was similar to the preparation process of Pd⁴⁺/MOL, except MOL sample (10 mg) was replaced by UiO-67-bpy (10 mg). Reduction processes: 10 mg Pd⁴⁺/UiO-67-bpy was dispersed in 3 mL water and 8 mg NaBH₄ in 1 mL water was dropwise added into mixture containing Pd⁴⁺/UiO-67-bpy, which was stirred for 3 h at room temperature. After washed by 5 mL deionized water for three times, Pd/UiO-67-bpy was obtained and dried in vacuum (yield ca. 10 mg).

2.2.5. Preparation of Pd/N-rGO

Graphene oxide (GO) was synthesized from graphite powder by Hummers method [43]. Nitrogen-doped reduced GO (N-rGO) was obtained according to the literature procedure [44]: 40 mg graphene oxide was heated to 800 °C with 3 °C min⁻¹ heating rate under NH₃ atmosphere. 10 mg N-rGO was dispersed in 3 mL water by sonication, and

50 μL K₂PdCl₆ solution (10 mg mL⁻¹) was added, which were stirred for 24 h at 800 rpm. After that, 1 mL NaBH₄ aqueous solution (8 mg) was added into the mixture and reacted at 25 °C for 3 h. The resulted precipitates were filtrated and dried for further use [45].

2.3. Physical characterization

Powder X-ray diffraction (PXRD) patterns were performed on Bruker D8 ADVANCE (40 kV tube voltage and 40 mA tube current). Thermogravimetric analysis (TGA) was determined by a HENVEN HTG-1 instrument and carried out flowing Ar or air atmosphere with the heating rate of 10 °C min⁻¹. Nitrogen sorption isotherms were measured by JW-BK200C (JWGB SCI.& TECH.) at the desired temperature (77 K). Samples were dried for 12 h at 423 K under vacuum before the nitrogen adsorption/desorption measurement. Valence state of element (Pd) was measured by X-ray photoelectron spectroscopy (XPS) on a K-Alpha⁺ X-ray photoelectron spectrometer (Thermo fisher Scientific) using an Al Kα source (12 kV, 6 mA). Scanning electron microscope (SEM) images were obtained using a SIGMA HD/VP analytical scanning electron microscope with acceleration voltage from 0.02 to 30 kV. All SEM samples were prepared by a deposition method, where samples were dispersed in ethanol, then loaded on a silicon substrate and heated at 60 °C. The size and morphologies of Pd/MOL was tested using a JEM-2100 F transmission electron microscope (TEM) and HRTEM working at 200 kV. Samples of Pd/MOL for SEM and TEM were fresh without any reaction, and catalytic recyclability samples of Pd/MOL for TEM and SEM were used after five times reactions. The contents of Pd and Zr in catalyst were quantified by inductively coupled plasma atomic emission spectroscopy (ICP-AES) on an IOAP6300 analyzer (PerkinElmer). Gas chromatographic (GC) analysis was carried out using a Lunan Ruihong SP-7820 instrument equipped with a flame ionization detector and a SE-54 column (length = 30 m, inner diameter = 0.32 mm, and film thickness = 0.50 μm). The products of catalytic reactions were analysed and identified by GC and proton nuclear magnetic resonance (¹H NMR) (Bruker 400 MHz Advance). The contact angle was measured by a Goniometer (using the sessile drop method at room temperature), supplied by M/s, Rame-Hart instrument Co., USA (model: 300 F4 series). The contact angle measurement was carried out using a LAUDA Scientific LSA100 instrument, and samples were prepared by pressing the mixture of 30 mg Pd/MOL (or Pd/N-rGO) and PTFE (2.5 wt%, to weaken the effect of capillarity on the contact angle) into a pellet under 10 MPa with a pelleting machine.

2.4. Hydrogenation procedures

2.4.1. General procedure of Route I

Hydrogenation reaction of CAL or other substrates following **Route I** was conducted in an open 25 mL PTFE-lined high-pressure autoclave. Generally, 4.8 mmol substrate and 1.6 mmol NH₃·BH₃ were dispersed in 5 mL water in the open autoclave and then the reaction was performed at 25 °C with 800 rpm for 15 min. The conversion and selectivity were calculated by ¹H NMR.

2.4.2. General procedure of Route II

Hydrogenation reaction of CAL or other substrates following **Route II** was conducted in a 25 mL autoclave with two different sizes of linings (as shown in Scheme 2). Generally, the outer is for hydrogenation of substrates, containing 4.8 mmol substrates and 10 mg Pd/MOL in 5 mL water, and the inner is for NH₃·BH₃ decomposition, containing 5 mg Pd/MOL and 4.86 mmol NH₃·BH₃ in 5 mL water. Before reaction, the autoclave was purged with H₂ four times at room temperature to remove air in autoclave. Then the reaction was performed at 80 °C and 800 rpm for 1 h, where the highest pressure arrived at ca. 1.05 MPa. After the reaction, in consideration of insolubility of various UALs in water, water phase containing organic products was extracted with 10 mL ethyl acetate, which was repeated for three times (the solid catalyst was

removed by centrifugation). The total extracted solution was mixed and condensed to 10 mL. The conversion and selectivity were calculated by ^1H NMR and GC with n-dodecane as an internal standard.

2.4.3. General procedure of Route III

Hydrogenation reaction of CAL or other substrates following **Route III** was conducted in a 25 mL PTFE-lined high-pressure autoclave. Generally, 4.8 mmol substrate and 6.5 mmol $\text{NH}_3\cdot\text{BH}_3$ were dispersed in 5 mL water in the sealed autoclave. The autoclave was purged with H_2 four times at room temperature to remove air in autoclave before reaction, and then the reaction was performed at 80°C with 800 rpm for a defined time depending on substrates. The conversion and selectivity were calculated by ^1H NMR.

3. Results and discussion

3.1. Structural and morphological characterizations of Pd/MOL

Precise control of selective hydrogenation of UALs is achieved by simply switching the roles of AB in transfer and/or catalytic hydrogenation, as illustrated in **Scheme 2**. Pd based catalyst is important for realizing this strategy since Pd not only tends to hydrogenate $\text{C}=\text{C}$ over $\text{C}=\text{O}$ but also *in situ* dehydrogenates AB to produce H_2 . MOL, as a kind of two-dimensional MOFs, serves an ideal support for immobilization of metal nanoparticles, which could expose active sites on the surface rather than into pores or channels in three-dimensional MOFs [46]. Therefore, Pd/MOL was adopted as a catalyst for dehydrogenation of AB and hydrogenation of $\text{C}=\text{C}$ bonds. Specifically, a microporous zirconium-based MOL with the chemical formula, $\text{Zr}_{12}(\mu_3\text{-O})_8(\mu_3\text{-OH})_8(\mu_2\text{-OH})_6(\text{BPYDC})_9$ was selected as the host to immobilize Pd nanoparticles, due to the large surface area, high stability in water, and coordination ability of BPYDC for dispersion of metal

nanoparticles. Pd/MOL was prepared by adsorption of Pd species with MOLs followed by reduction with NaBH_4 (**Fig. S1**).

Morphology of Pd/MOL was characterized by SEM and TEM as shown in **Fig. 1a-c**. Typical SEM image (**Fig. 1a**) reveals that Pd/MOL is present as nanosheets with breadth of ca. 250 nm and thickness of ca. 25 nm. TEM images demonstrate that the Pd nanoparticles have excellent dispersion with an average size of ca. 4.2 nm (**Fig. 1c**). The loading of Pd within Pd/MOL, Pd/UiO-67-bpy and Pd/N-rGO were 1.44 wt%, 2.91 wt% and 2.07 wt%, respectively, measured by ICP-MS. The loading of Pd can be increased by adding more K_2PdCl_6 during the synthesis (**Fig. S3e**). The PXRD demonstrates that the composites remain the original crystal structure of MOL after adsorption of Pd^{4+} and loading of Pd nanoparticles (**Fig. 1d**). In addition, no obvious diffraction peak of Pd nanoparticles was observed (PDF#65–6174), indicative of the formation of small Pd nanoparticles or/and low metal content in Pd/MOL. XPS spectra of Pd/MOL and MOL are shown in **Fig. S2d and S6**. N 1 s peak at 398.9 eV for pure MOL corresponds to uncoordinated N of BPYDC in MOL. After loading Pd nanoparticles, the N 1 s peak shifts to 400.7 eV, revealing the presence of strong interaction between BPYDC and Pd nanoparticles in Pd/MOL, due to the decrease in electron density of N [47]. Moreover, **Fig. S2d** demonstrates that a Pd $3d_{5/2}$ band at ca. 335–336 eV in Pd/MOL, corresponding to a typical Pd metal, which indicates that the Pd^{4+} cations were reduced to Pd(0) after addition of NaBH_4 [47,48]. The specific surface areas of as-synthesized pure MOL and Pd/MOL are 666 and $531\text{ m}^2\text{ g}^{-1}$, respectively, as calculated from nitrogen sorption isotherms (**Fig. S2c**). The slight decrease of the specific surface area may suggest that parts of pores of MOL were occupied by low loading of Pd nanoparticles, consistent with the TEM image. TGA of MOL and Pd/MOL was carried out, which shows that catalysts would be durable in the following experiments (**Fig. S2a and S2b**) [40].

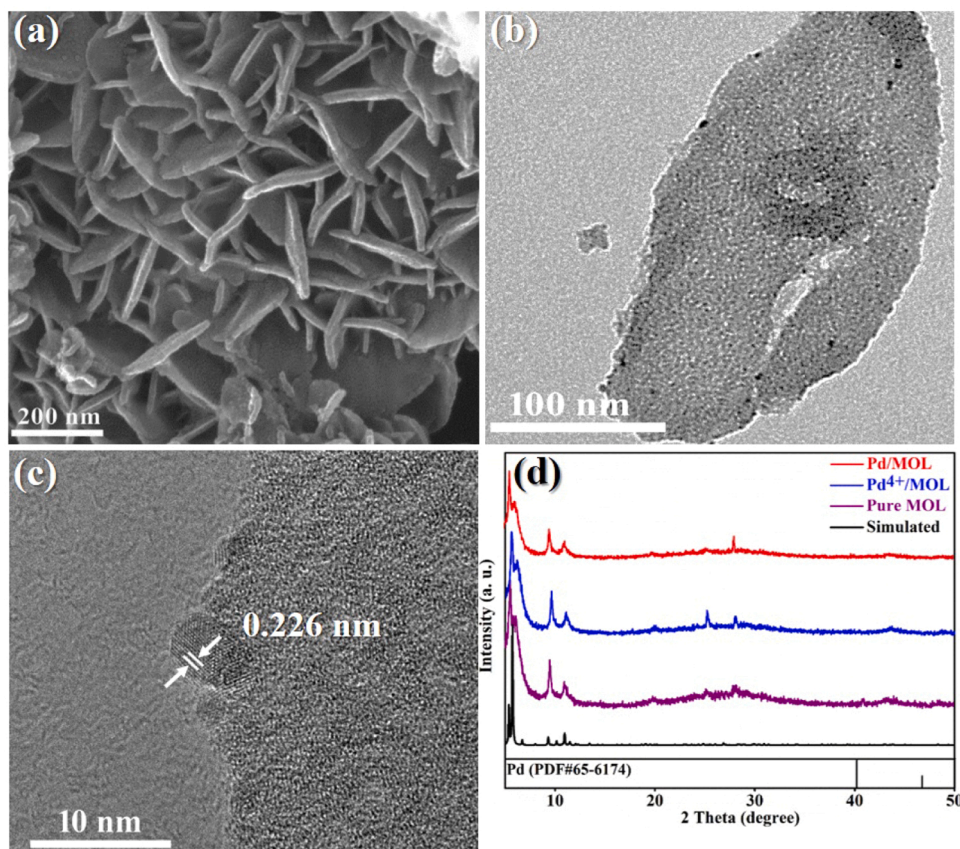


Fig. 1. SEM (a), TEM (b), and HRTEM (c) images of Pd/MOL and (d) PXRD patterns of Pd/MOL, Pd^{4+} /MOL, and pure MOL.

3.2. Hydrogenation of α,β -unsaturated aldehydes

Precise control of selective hydrogenation of UALs is of significant importance for their practical applications. Scheme 2 shows that three routes (I, II, and III) can be employed to regulate the hydrogenation selectivity of UALs via flexible utilization of AB and Pd/MOL. We first selected hydrogenation of CAL as a model reaction to evaluate the hydrogenation performances in different routes. The effect of reaction conditions on hydrogenation performance of AB in water was investigated by mixing CAL and AB in an open autoclave under diverse conditions: molar ratios of AB and CAL (1:1–1:6), reaction temperatures (25–100 °C), and reaction time (15 min to 3 h) (Fig. 2). It is found that C=O bonds can be exclusively hydrogenated with AB in the neat water under very mild conditions (room temperature for 15 min under air condition; various transfer-hydrogenation strategies are shown in Table S1 for comparison). The optimal molar ratio of AB and CAL is 1:3 (Fig. 2c), which matches very well with the theoretical value, indicative of the very high hydrogenation efficiency of AB. Therefore, COL can be efficiently produced with extremely high conversion and selectivity under very mild conditions (Figs. 2a and b, Route I).

To identify the hydrogenation route, we further carried out a control experiment, that is, attempting to decompose AB without any catalyst. No dehydrogenation phenomenon of AB was observed under different reaction conditions (Fig. S7b), even though the reaction temperature and time were raised to 100 °C and 3 h, respectively, which excludes the catalytic hydrogenation mechanism. Therefore, the transfer hydrogenation mechanism should be responsible for selective hydrogenation of CAL into COL [37,49–51]. To verify the universality of Route I for UAL hydrogenation, a series of UALs with various substitute groups (including 4-methylphenyl, 4-fluorophenyl, 4-bromophenyl, 4-methoxyphenyl, dimethyl, or ethyl groups) were hydrogenated under above optimized conditions. As shown in Fig. 2d, in all cases, diverse substrates

were exclusively converted to related UOLs with 100% selectivity by AB in water for 15 min at room temperature. These results indicate that AB can exclusively reduce C=O bonds of UOLs rather than C=C bonds.

Selective hydrogenation of C=C bonds was achieved following the Route II in Scheme 2, where selection of Pd/MOL as the catalyst is a critical step. Pd/MOL not only shows high hydrogenation selectivity towards C=C bonds but also dehydrogenates AB to release H₂ for catalytic hydrogenation, so that to hydrogenate C=C bonds without using additional high-pressure H₂-source. To avoid transfer hydrogenation of C=O bonds with AB, selective hydrogenation of C=C bonds in CAL was conducted in a 25 mL autoclaves with two different sizes of linings, where the inner contained Pd/MOL and AB in water for AB decomposition and the outer contained CAL and Pd/MOL in water for hydrogenation of substrates. The effect of reaction temperature, time and amount of AB on CAL conversion and HCAL selectivity was evaluated to optimize the reaction conditions. The effect of the reaction temperature was first investigated with 4.86 mmol AB for 1 h (Fig. 3a) (The relationship between the amount of AB and H₂ pressure is shown in Fig. S8).

The CAL conversion increases from 8.1% to 100% with the temperature increasing from 25° to 80 °C. CAL conversion strongly depends on the temperature, because the hydrogenation of C=C in CAL is a thermodynamically favorable process. The conversion reaches 100% at 80 °C with 92% HCAL selectivity, but no COL was detected despite of further increasing the temperature to 110 °C, indicating that the Pd/MOL catalyst is almost inactive for hydrogenation of C=O when competing with C=C bonds. The effect of reaction time was then assessed with 4.86 mmol AB at 80 °C. As revealed in Fig. 3b, increasing the reaction time from 20 min to 1 h leads to a rapid increase in CAL conversion from 32% to 100% and further increasing the reaction time results in a slight decrease of HCAL selectivity because of the further hydrogenation of HCAL to HCOL. The amount of AB actually reflects the pressure of *in situ* produced H₂, which is an important parameter to

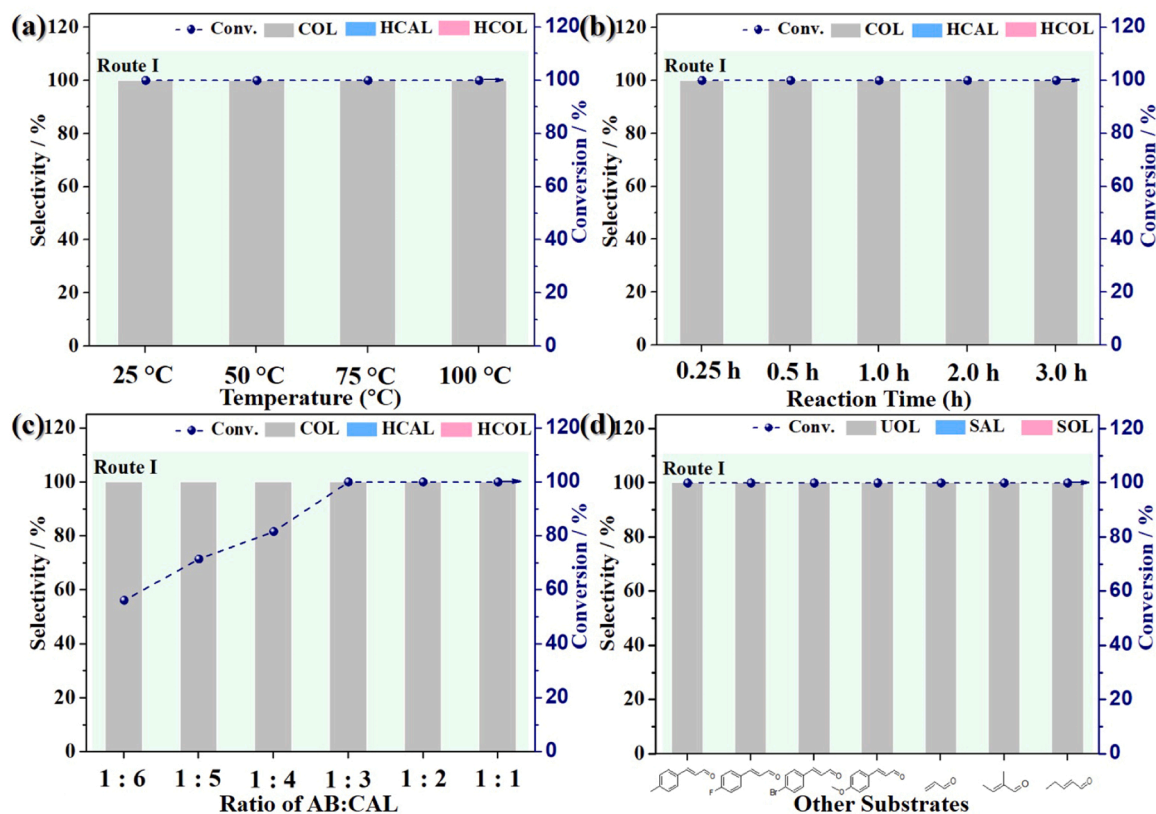


Fig. 2. Effect of reaction temperature (15 min, AB:CAL = 1:3) (a), reaction time (25 °C, AB:CAL = 1:3) (b), and molar ratio (25 °C, 15 min) (c) on CAL conversion and COL selectivity; (d) Extension of exclusive hydrogenation to different substrates (25 °C, 15 min, AB:CAL = 1:3). Same reaction conditions: 4.8 mmol substrates, 5 mL H₂O, 800 rpm.

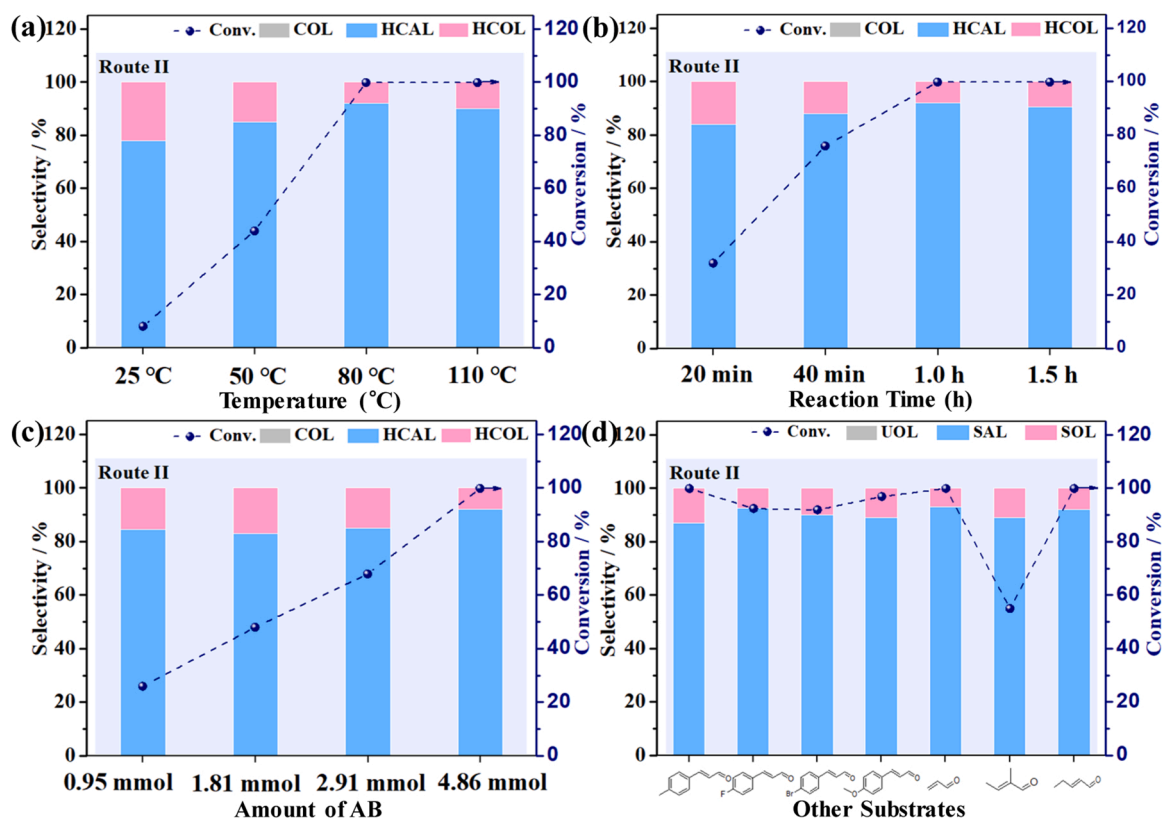


Fig. 3. Effect of reaction temperature (1 h, 4.86 mmol AB) (a), reaction time (80 °C, 4.86 mmol AB) (b), and amount of AB (1 h, 80 °C) (c) on CAL conversion and HCAL selectivity; (d) Extension of selective hydrogenation to different substrates (1 h, 80 °C, 4.86 mmol AB). Same reaction conditions: Pd/MOL (0.144 mg Pd, for catalytic hydrogenation), substrates (4.8 mmol), water (5 mL), 800 rpm.

influence the conversion. The dependent on the amount of AB was investigated at 80 °C for 1 h (Fig. 3c). An increase in the amount of AB from 0.95 to 4.86 mmol leads to an increase of CAL conversion from 26% to 100% and HCAL selectivity from 84% to 92%.

Impressively, Pd/MOL demonstrates outstanding hydrogenation efficiency for CAL conversion to HCAL, as compared with several control samples: including MOL, Pd nanoparticles, Pd/C, Pd/N-rGO and Pd/UiO-67-bpy. These materials were characterized by XRD, SEM and TEM (Fig. S3-S5). Pd/MOL reaches 100% CAL conversion and 92% HCAL selectivity and turnover frequency (TOF) of CAL as high as 0.98 s^{-1} at 1 h (Table 1), amongst the highest active catalysts for selective hydrogenation of CAL into HCAL (Table S5). The reaction rate could be further increased by increasing the loading of Pd within the composites. The conversion can arrive at 100% with 90% selectivity within 15 min using 8.2 wt% Pd/MOL as the catalyst (Fig. S9a). Comparing results indicate that Pd/MOL with 1.44 wt% of Pd has higher TOF value and Pd atomic efficiency than those of 8.2 wt% Pd (Fig. S9b). Control experiments with pure MOL as the catalyst or without any catalyst show extremely low conversion, indicating Pd is the active site for hydrogenation reaction. On the contrary, Pd, Pd/C, Pd/N-rGO and Pd/UiO-67-bpy show much lower conversion and TOF values following the order: Pd/MOL (0.98 s^{-1}) > Pd/C (0.68 s^{-1}) > Pd/N-rGO (0.62 s^{-1}) > Pd/UiO-67-bpy (0.51 s^{-1}) > Pd nanoparticles (0.42 s^{-1}). To verify the universality of Route II, similar reaction conditions were applied for hydrogenation of UALs with different substituents. As shown in Fig. 3d, almost all the substrates can achieve over 90% conversion after 1.0 h, accompanied by ca. 90% SAL selectivity. As for 2-methyl-2-butenal, 55% conversion were reached under the standard conditions with 90% of SAL selectivity possibly because of the steric hindrance of the methyl group. The TOF values of hydrogenation of various UALs by Pd/MOL are shown in Table 1, S2 and S5, which are much higher than those in the reported work [32,47,52–55].

Table 1

Catalytic performance of various Pd based catalysts in Route II.

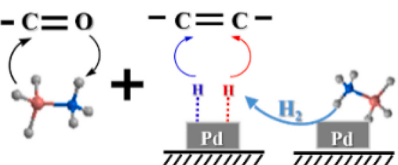
Entry	Catalyst	t (h)	Conv. (%)	Sel. (%)			TOF (s^{-1})
				HCAL	COL	HCOL	
1	–	1.0	2	30	0	70	–
2	MOL	1.0	1.5	17	0	83	–
3	Pd NPs	1.0	42	84	0	16	0.42
4	Pd/MOL	1.0	100	92	0	8	0.98
5	Pd/C	1.0	69	89	0	11	0.68
6	Pd/N-rGO	1.0	62	88	0	12	0.61
7	Pd/UiO-67-bpy	1.0	52	93	0	7	0.51

Reaction conditions: Pd/MOL (0.144 mg Pd, for catalytic hydrogenation), CAL (0.6 mL, 4.8 mmol); water (5 mL), temperature (80 °C), 4.86 mmol AB, 800 rpm. TOF was calculated as quantity of substrates converted per mole number of total Pd per second. Catalytic reaction products were determined by GC and ^1H NMR.

The complete hydrogenation product, HCOL was obtained by transfer hydrogenation along with catalytic hydrogenation using Pd/MOL and AB together (Table 2 and S3, Route III). Pd/MOL was introduced as the catalyst and AB as both the hydrogen donor for transfer hydrogenation and hydrogen source for catalytic hydrogenation. CAL was converted completely to HCOL without any by-product. Control experiments were carried out with pure MOL, Pd nanoparticles, Pd/C

Table 2

Complete hydrogenation of various UALs into corresponding SOLs over Pd/MOL and AB following **Route III**.



Entry	Substrate	Conv. (%)	t (h)	AB (mmol)	Sel. (%)		
					SAL	UOL	SOL
1		100	3.21	6.5	0	0	100
2		100	3.25	6.5	0	0	100
3		100	3.75	6.5	0	0	100
4		100	3.25	6.5	0	0	100
5		100	3.75	6.5	0	0	100
6 ^c		100	3.25	6.5	0	0	100
7		100	5.5	11.3	0	0	100
8		100	3.25	6.5	0	0	100

Reaction conditions: Pd/MOL (0.144 mg Pd), substrate (4.8 mmol); water (5 mL), temperature (80 °C), 800 rpm. Catalytic reaction products were determined by ¹H NMR.

and Pd/Uio-67-bpy as catalysts or without any catalyst. The control experiments show the similar results with those in **Route II**, where Pd is the active species and COL conversion and HCOL selectivity exhibited the following order: Pd/MOL > Pd/C > Pd nanoparticles ≈ Pd/Uio-67-bpy. This strategy is also applicable for complete hydrogenation of various UALs into corresponding SOLs (**Table 2** in **Route III**). The activity of Pd/MOL toward C=C hydrogenation was affected by variation of substitutes, because of the steric and/or electronic effects. However, complete conversion and 100% SOL selectivity were still achieved by increasing the reaction time and/or the amount of AB (as shown in **Table 2**). Much longer reaction time was required to accomplish the hydrogenation, possibly because that the same amount of Pd/MOL was used as that in catalytic hydrogenation in **Route II**, but Pd/MOL simultaneously decompose AB and catalytically hydrogenate C=C bonds in **Route III**.

The stability and recyclability of as-prepared Pd/MOL are important for their further industrial applications, which were examined by consecutive reactions as characterized by SEM, TEM and powder XRD (**Fig. S10**). The recyclability experiments of **Route II** and **III** were conducted under the same conditions, and the Pd/MOL catalyst was recycled by repeated centrifugation and wash with ethyl acetate. As shown in **Fig. S11a** and **S11b**, Pd/MOL almost retains the selectivity and conversion for CAL hydrogenation after six consecutive runs, and the slight decrease after 4 consecutive runs is mainly because of loss of Pd/MOL during the separation process. The satisfactory stability and recyclability were attributed to two reasons: (i) The micropore confinement in MOL can effectively prevent the aggregation of Pd nanoparticles; (ii) The coordination ability of N in the BPYDC ligand has strong interaction with Pd nanoparticles to ensure that Pd was anchored in MOL. Moreover, Pd nanoparticles within the catalyst was not significantly aggregated after six runs, as shown by TEM and HRTEM images of Pd/MOL (**Fig. S10c** and **S10d**). The SEM image and powder XRD patterns (**Fig. S10a** and **S10b**) demonstrated that the structure and morphology were retained after reactions, and the Pd nanoparticles were still well-dispersed. The ICP result shows no detectable leaching of Pd during the reaction. The excellent recyclability may result from the ordered micropores of MOL and strong interactions originated from the BPYDC

ligand, which could confine and disperse the Pd nanoparticles.

The above-mentioned results (**Route I-III**) demonstrate that the hydrogenation selectivity of UALs can be precisely controlled in the water by simply switching the roles of AB for transfer and/or catalytic hydrogenation. Exclusive hydrogenation of C=O in UALs to UOLs was achieved merely with AB through the transfer hydrogenation. Selective hydrogenation of C=C in UALs to SALs was realized using Pd/MOL as the catalyst and *in situ* released H₂ as hydrogen source through the catalytic hydrogenation. Complete hydrogenated products can be exclusively produced using AB and Pd/MOL together through transfer hydrogenation along with catalytic hydrogenation. During these hydrogenation processes, AB represents irreplaceable functions for UAL hydrogenation to synthesize three reduced products: i) hydrogen donor for C=O transfer hydrogenation and ii) hydrogen source for C=C catalytic hydrogenation.

To deeply understand the exclusive hydrogenation of CAL with AB, Fourier transform infrared (FT-IR) spectra for CAL, COL, AB and mixture of AB and CAL were measured as shown in **Fig. S12a**. The absorbance of C=O stretching vibration peak in pure CAL was situated at around 1672 cm⁻¹, but this characteristic peak disappeared within 5 min after addition of AB, indicating the rapid reduction of CAL by AB. Density functional theory (DFT) simulation was further performed to reveal the mechanism of the exclusive hydrogenation of C=O bonds by AB. It is found that AB is inclined to approach the C=O bond forming a six-membered ring structure (**Fig. 4a** and **S12b**), even though AB was initially located close to the C=C bond but far away from C=O bonds. This indicates that the strong interaction is present between AB and C=O, which explains the reason of exclusive reduction for C=O bonds. Chen et al. [56,57] employed isotopic labeling experiments to reveal that a double hydrogen transfer process was underwent for reduction of C=O in benzaldehyde by AB. Inspired by this work, we proposed a reaction route for exclusive reduction of CAL by AB (**Fig. S12b**). Initially, protic H_a and hydridic H_b in AB were transferred to oxygen and carbon end of carbonyl in CAL, respectively (process 1 in **Fig. S12b**). After that, AB was converted into the very reactive [H₂B=NH₂] molecule, which further aggregated into cyclotriborazane (CTB) or B-(cyclodiborazany) aminoborohydride (BCDB) (process 2 in **Fig. S12b**), confirmed by Berke et al. [33] CTB and BCDB could further reduce CAL to COL, with polyborazylene and borazine as byproducts, respectively (process 3 in **Fig. S12b**). Totally, 1 mol AB can reduce the 3 mol C=O in CAL, corresponding to the theoretic hydrogen storage capacity of AB (process 4 in **Fig. S12b**). To explore the reason for high selectivity of Pd/MOL towards hydrogenation of C=C bonds in UAL, the COL and HCOL were hydrogenated with Pd/MOL, respectively (**Fig. S12c**). COL could be completely hydrogenated to HCOL after 1.0 h, however, HCOL was hardly converted to HCOL under the same conditions. These results confirm that Pd/MOL are active toward C=C hydrogenation, but almost inert toward C=O hydrogenation, leading to high selectivity of CAL to HCOL. The high selectivity of Pd towards hydrogenation of C=C bonds could be explained by a planar η⁴ mode (**Fig. S12d**) as a favorable adsorption orientation for the CAL molecule, which leads to preferential formation of HCOL, as confirmed by the DFT simulation in Delbecq's work [58].

To reveal the excellent catalytic activity of Pd/MOL, we further compared the catalytic performances of several control samples (**Table 1**) and investigated the dispersibility of Pd-based catalysts. We first compared the catalytic performances between Pd/MOL and Pd/Uio-66-bpy, where both catalysts are formed with the same compositions but different topologies (the former is nanosheet and the latter is three-dimensional). Pd/MOL shows obviously higher catalytic activity than Pd/Uio-67-bpy (TOF values are 0.98 and 0.51 s⁻¹, respectively). This demonstrates the nanosheet structure of the support is beneficial for improving the catalytic activity because of more exposed active sites and faster mass transfer efficiency. The catalytic performances between Pd/MOL and Pd/N-rGO were compared, where both MOL and N-rGO are two-dimensional. Pd/MOL still shows higher catalytic activity than Pd/

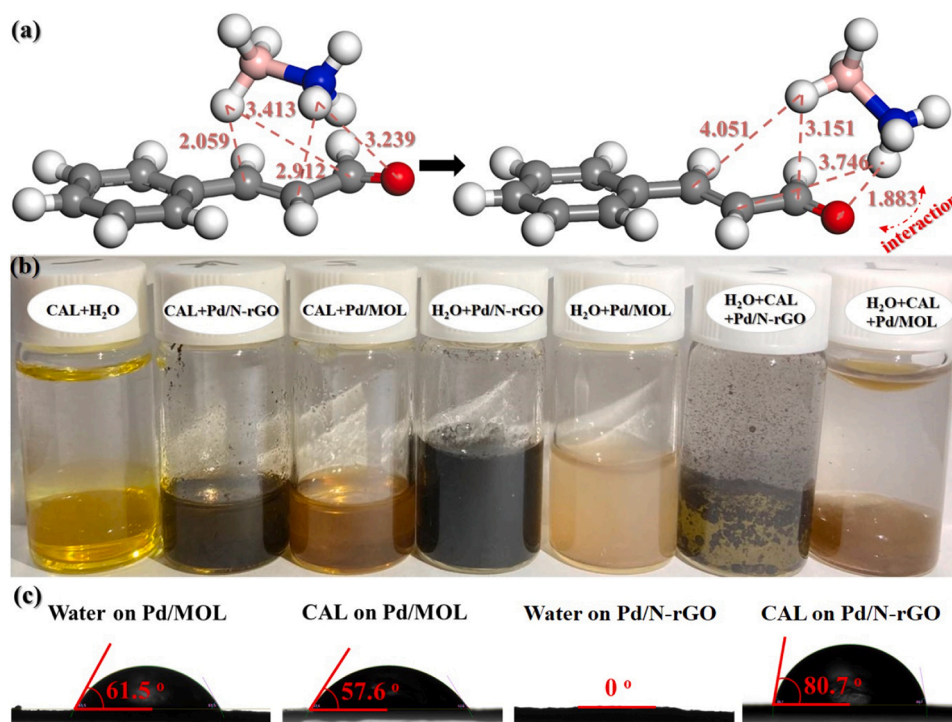


Fig. 4. (a) Default structure between AB and CAL by DFT simulation; (b) Photos of Pd/MOL and Pd/N-rGO dispersed in CAL, water, and mixture of CAL+H₂O, respectively; (c) Contact angles of water or CAL drop on Pd/MOL or Pd/N-rGO pellet (with 2.5 wt% PTFE).

N-rGO (TOF values are 0.98 and 0.62 s⁻¹, respectively). Since both supports are two-dimensional, we propose that the higher activity may arise from the different surface property of two supports. Thus, the dispersibility in different solvents (water, CAL, and mixture of CAL and H₂O) were investigated for Pd/MOL and Pd/N-rGO. As shown in Fig. 4b, Pd/MOL can be well dispersed in both water and CAL; contrarily, Pd/N-rGO tends to disperse in water than CAL. Therefore, Pd/MOL is still dispersed between the interface of H₂O and CAL but Pd/N-rGO aggregates for the mixture solvents. This phenomenon can be well understood by the amphipathicity nature of MOL [59] and hydrophilicity for N-rGO, which can be further confirmed by the contact angle measurement of water or CAL drop on Pd/MOL or Pd/N-rGO (Fig. 4c). Therefore, the high catalytic efficiency of Pd/MOL may be ascribed to the unique layer porous structure of MOL with more exposed active sites and improved mass transfer efficiency, and amphipathicity nature of MOL with better affinity to CAL and H₂O.

4. Conclusion

In summary, we have successfully employed AB as a mediator to precisely control the selective hydrogenation of UALs in water under mild conditions. UOLs can be exclusively produced by AB via transfer hydrogenation. SALs are selectively prepared using Pd/MOL as the catalyst together with *in situ* release of H₂ from AB. SOLs can be readily synthesized with AB and Pd/MOL by a combination of transfer and catalytic hydrogenation. The exclusive hydrogenation of C=O bonds of AB is associated with the strong interaction between AB and C=O bonds instead of C=C bonds. Moreover, Pd/MOL shows very high catalytic activity for hydrogenation of UALs into SALs because of the unique porous layered structure and amphipathic nature of MOL. The catalytic system can be widely extended to various UAL hydrogenation with high conversion and selectivity, which may be adaptable for hydrogenation of other intricate compounds with both unpolarized and polarized (such as polar olefins, ketones, nitro, and imine) unsaturated bonds. This work not only provides a skillful approach for precise control of hydrogenation selectivity of intricate compounds with competing unsaturated

bonds, but also achieves the hydrogenation under sustainable conditions avoiding the use of organic solvents and extra high-pressure hydrogen source.

CRediT authorship contribution statement

J. Huo: Conceived the conceptualization. **Z. Zeng:** Conceived the conceptualization. **Y. Zhou:** Performed the synthesis, Characterizations, and catalytic tests. **C. Chen:** Conducted part of the synthesis of catalysts and characterizations. **Q. Li:** Conducted part of the synthesis of catalysts and characterizations. **Y. Liu:** Conducted part of the synthesis of catalysts and characterizations. **T. Wei:** Conducted part of the synthesis of catalysts and characterizations. **Y. Liu:** Conducted part of the synthesis of catalysts and characterizations. The manuscript was primarily written by Y. Zhou, and revised by J. Huo, D. Bradshaw and Z. Zeng. All authors discussed the results and commented on the manuscript.

Declaration of Competing Interest

The authors declare that they have no known competing financial interests or personal relationships that could have appeared to influence the work reported in this paper.

Acknowledgements

This work was supported by the National Natural Science Foundation of China (Grant No: 2217809022178090, 2157306321573063), the Hunan Provincial Natural Science Fund for Excellent Young Scholars (2020JJ3002), Open Fund from Hunan Provincial Key Laboratory of Advanced Materials for New Energy Storage and Conversion (Grant No: 2018TP1037_201902), Hunan University Training Program for Excellent Young Scholars, and Shenzhen Science and Technology Program (Grant No. RCJC20200714114434015).

Appendix A. Supporting information

Supplementary data associated with this article can be found in the online version at [doi:10.1016/j.apcatb.2022.121348](https://doi.org/10.1016/j.apcatb.2022.121348).

References

- [1] Y. Yang, Z. Ren, S. Zhou, M. Wei, Perspectives on multifunctional catalysts derived from layered double hydroxides toward upgrading reactions of biomass resources, *ACS Catal.* 11 (2021) 6440–6454, <https://doi.org/10.1021/acscatal.1c00699>.
- [2] W. Liu, Y. Yang, L. Chen, E. Xu, J. Xu, S. Hong, X. Zhang, M. Wei, Atomically-ordered active sites in NiMo intermetallic compound toward low-pressure hydrodeoxygenation of furfural, *Appl. Catal. B Environ.* 282 (2021), 119569, <https://doi.org/10.1016/j.apcatb.2020.119569>.
- [3] Q. Liu, Q. Liu, Y. Chen, Y. Li, H. Su, Q. Liu, G. Li, Ir nanoclusters confined within hollow MIL-101(Fe) for selective hydrogenation of α,β -unsaturated aldehyde, *Chin. Chem. Lett.* 33 (2022) 374–377, <https://doi.org/10.1016/j.ccl.2021.06.047>.
- [4] X. Zhang, H. Liu, Y. Shi, J. Han, Z. Yang, Y. Zhang, C. Long, J. Guo, Y. Zhu, X. Qiu, G. Xue, L. Zhang, B. Zhang, L. Chang, Z. Tang, Boosting CO₂ conversion with terminal alkynes by molecular architecture of graphene oxide-supported Ag nanoparticles, *Matter* 3 (2020) 558–570, <https://doi.org/10.1016/j.matt.2020.07.022>.
- [5] M. Crespo-Quesada, F. Cárdenas-Lizana, A.L. Dessimoz, L. Kiwi-Minsker, Modern trends in catalyst and process design for alkyne hydrogenations, *ACS Catal.* 2 (2012) 1773–1786, <https://doi.org/10.1021/cs300284r>.
- [6] F. Meemken, A. Baiker, Recent progress in heterogeneous asymmetric hydrogenation of C=O and C=C bonds on supported noble metal catalysts, *Chem. Rev.* 117 (2017) 11522–11569, <https://doi.org/10.1021/acs.chemrev.7b00272>.
- [7] L. Zhang, M. Zhou, A. Wang, T. Zhang, Selective hydrogenation over supported metal catalysts: from nanoparticles to single atoms, *Chem. Rev.* 120 (2020) 683–733, <https://doi.org/10.1021/acs.chemrev.9b00230>.
- [8] J. Guo, Y. Qin, Y. Zhu, X. Zhang, C. Long, M. Zhao, Z. Tang, Metal-organic frameworks as catalytic selectivity regulators for organic transformations, *Chem. Soc. Rev.* 50 (2021) 5366–5396, <https://doi.org/10.1039/D0CS01538E>.
- [9] X. Wang, X. Liang, P. Geng, Q. Li, Recent advances in selective hydrogenation of cinnamaldehyde over supported metal-based catalysts, *ACS Catal.* 10 (2020) 2395–2412, <https://doi.org/10.1021/acscatal.9b05031>.
- [10] R.R. Li, W.B. Yao, Y.X. Jin, W.P. Jia, X.Y. Chen, J.J. Chen, J.L. Zheng, Y. Hu, D. M. Han, J. Zhao, Selective hydrogenation of the C=C bond in cinnamaldehyde over an ultra-small Pd-Ag alloy catalyst, *Chem. Eng. J.* 351 (2018) 995–1005, <https://doi.org/10.1016/j.cej.2018.06.146>.
- [11] Y. Feng, W. Xu, B. Huang, Q. Shao, L. Xu, S. Yang, X. Huang, On-demand, ultraselective hydrogenation system enabled by precisely modulated Pd-Cd nanocubes, *J. Am. Chem. Soc.* 142 (2020) 962–972, <https://doi.org/10.1021/jacs.9b10816>.
- [12] M. Zhao, K. Yuan, Y. Wang, G. Li, J. Guo, L. Gu, W. Hu, H. Zhao, Z. Tang, Metal-organic frameworks as selectivity regulators for hydrogenation reactions, *Nature* 539 (2016) 76–80, <https://doi.org/10.1038/nature19763>.
- [13] D. Wu, W. Baaziz, B. Gu, M. Marinova, W.Y. Hernández, W. Zhou, E.I. Vovk, O. Ersen, O.V. Safonova, A. Addad, N. Nuns, A.Y. Khodakov, V.V. Ordonsky, Surface molecular imprinting over supported metal catalysts for size-dependent selective hydrogenation reactions, *Nat. Catal.* 4 (2021) 595–606, <https://doi.org/10.1038/s41929-021-00649-3>.
- [14] X. Yang, J.K. Sun, M. Kitta, H. Pang, Q. Xu, Encapsulating highly catalytically active metal nanoclusters inside porous organic cages, *Nat. Catal.* 1 (2018) 214–220, <https://doi.org/10.1038/s41929-018-0030-8>.
- [15] X. Lan, T. Wang, Highly selective catalysts for the hydrogenation of unsaturated aldehydes: a review, *ACS Catal.* 10 (2020) 2764–2790, <https://doi.org/10.1021/acscatal.9b04331>.
- [16] H. Wang, S. Bai, Y. Pi, Q. Shao, Y. Tan, X. Huang, A strongly coupled ultrasmall Pt₃Co nanoparticle-ultrathin Co(OH)₂ nanosheet architecture enhances selective hydrogenation of α,β -unsaturated aldehydes, *ACS Catal.* 9 (2018) 154–159, <https://doi.org/10.1021/acscatal.8b03471>.
- [17] R. Gao, L. Pan, H. Wang, Y. Yao, X. Zhang, L. Wang, J.J. Zou, Breaking trade-off between selectivity and activity of nickel-based hydrogenation catalysts by tuning both steric effect and d-band center, *Adv. Sci.* 6 (2019), 1900054, <https://doi.org/10.1002/adv.201900054>.
- [18] Y. Lv, M. Han, W. Gong, D. Wang, C. Chen, G. Wang, H. Zhang, H. Zhao, Fe-Co alloyed nanoparticles catalyzing efficient hydrogenation of cinnamaldehyde to cinnamyl alcohol in water, *Angew. Chem. Int. Ed.* 59 (2020) 23521–23526, <https://doi.org/10.1002/anie.202009913>.
- [19] Y. Zhu, H. Qian, B.A. Drake, R. Jin, Atomically precise Au₂₅(SR)₁₈ nanoparticles as catalysts for the selective hydrogenation of α,β -unsaturated ketones and aldehydes, *Angew. Chem. Int. Ed.* 49 (2010) 1295–1298, <https://doi.org/10.1002/anie.200906249>.
- [20] B. Wu, H. Huang, J. Yang, N. Zheng, G. Fu, Selective hydrogenation of α,β -unsaturated aldehydes catalyzed by amine-capped platinum-cobalt nanocrystals, *Angew. Chem. Int. Ed.* 51 (2012) 3440–3443, <https://doi.org/10.1002/anie.201108593>.
- [21] Y. Dai, X. Gao, X. Chu, C. Jiang, Y. Yao, Z. Guo, C. Zhou, C. Wang, H. Wang, Y. Yang, On the role of water in selective hydrogenation of cinnamaldehyde to cinnamyl alcohol on PtFe catalysts, *J. Catal.* 364 (2018) 192–203, <https://doi.org/10.1016/j.jcat.2018.05.008>.
- [22] G. Wang, H. Xin, Q. Wang, P. Wu, X. Li, Efficient liquid-phase hydrogenation of cinnamaldehyde to cinnamyl alcohol with a robust PtFe/HPZSM-5 catalyst, *J. Catal.* 382 (2020) 1–12, <https://doi.org/10.1016/j.jcat.2019.12.004>.
- [23] C.M. Piqueras, V. Puccia, D.A. Vega, M.A. Volpe, Selective hydrogenation of cinnamaldehyde in supercritical CO₂ over Me-CeO₂ (Me = Cu, Pt, Au): insight of the role of Me-Ce interaction, *Appl. Catal. B: Environ.* 185 (2016) 265–271, <https://doi.org/10.1016/j.apcatb.2015.12.031>.
- [24] J. Yu, Y. Yang, L. Chen, Z. Li, W. Liu, E. Xu, Y. Zhang, S. Hong, X. Zhang, M. Wei, NiBi intermetallic compounds catalyst toward selective hydrogenation of unsaturated aldehydes, *Appl. Catal. B: Environ.* 277 (2020), 119273, <https://doi.org/10.1016/j.apcatb.2020.119273>.
- [25] H. Liu, L. Chang, L. Chen, Y. Li, Nanocomposites of platinum/metal-organic frameworks coated with metal-organic frameworks with remarkably enhanced chemoselectivity for cinnamaldehyde hydrogenation, *ChemCatChem* 8 (2016) 946–951, <https://doi.org/10.1002/cctc.201501256>.
- [26] L. Jiao, J. Wang, H.L. Jiang, Microenvironment modulation in metal-organic framework-based catalysis, *Acc. Mater. Res.* 2 (2021) 327–339, <https://doi.org/10.1021/accountsmr.1c00009>.
- [27] D. Chen, W. Yang, L. Jiao, L. Li, S.H. Yu, H.L. Jiang, Boosting catalysis of Pd nanoparticles in MOFs by pore wall engineering: the roles of electron transfer and adsorption energy, *Adv. Mater.* (2020), e2000041, <https://doi.org/10.1002/adma.202000041>.
- [28] Q. Yang, Q. Xu, S.H. Yu, H.L. Jiang, Pd nanocubes@ZIF-8: Integration of plasmon-driven photothermal conversion with a metal-organic framework for efficient and selective catalysis, *Angew. Chem. Int. Ed.* 55 (2016) 3685–3689, <https://doi.org/10.1002/ange.201510655>.
- [29] L. Li, Z. Li, W. Yang, Y. Huang, G. Huang, Q. Guan, Y. Dong, J. Lu, S.H. Yu, H. L. Jiang, Integration of Pd nanoparticles with engineered pore walls in MOFs for enhanced catalysis, *Chem* 7 (2021) 686–698, <https://doi.org/10.1016/j.chempr.2020.11.023>.
- [30] K. Yuan, T. Song, D. Wang, X. Zhang, X. Gao, Y. Zou, H. Dong, Z. Tang, W. Hu, Effective and selective catalysts for cinnamaldehyde hydrogenation: Hydrophobic hybrids of metal-organic frameworks, metal nanoparticles, and micro- and mesoporous polymers, *Angew. Chem. Int. Ed.* 57 (2018) 5708–5713, <https://doi.org/10.1002/anie.201801289>.
- [31] W. Zhang, W. Shi, W. Ji, H. Wu, Z. Gu, P. Wang, X. Li, P. Qin, J. Zhang, Y. Fan, T. Wu, Y. Fu, W. Zhang, F. Huo, Microenvironment of MOF channel coordination with Pt NPs for selective hydrogenation of unsaturated aldehydes, *ACS Catal.* 10 (2020) 5805–5813, <https://doi.org/10.1021/acscatal.0c00682>.
- [32] H. Liu, Z. Li, Y. Li, Chemoselective hydrogenation of cinnamaldehyde over a Pt-Lewis acid collaborative catalyst under ambient conditions, *Ind. Eng. Chem. Res.* 54 (2015) 1487–1497, <https://doi.org/10.1021/ie504357r>.
- [33] X. Yang, L. Zhao, T. Fox, Z.X. Wang, H. Berke, Transfer hydrogenation of imines with ammonia-borane: a concerted double-hydrogen-transfer reaction, *Angew. Chem. Int. Ed.* 49 (2010) 2058–2062, <https://doi.org/10.1002/anie.200906302>.
- [34] F. Fu, C. Wang, Q. Wang, A.M. Martínez-Villacorta, A. Escobar, H. Chong, X. Wang, S. Moya, L. Salmon, E. Fouquet, J. Ruiz, D. Astruc, Highly selective and sharp volcano-type synergistic Ni₂Pt@ZIF-8-Catalyzed hydrogen evolution from ammonia borane hydrolysis, *J. Am. Chem. Soc.* 140 (2018) 10034–10042, <https://doi.org/10.1021/jacs.8b06511>.
- [35] H. Goksu, Y. Yildiz, B. Çelik, M. Yazici, B. Kilbas, F. Sen, Eco-friendly hydrogenation of aromatic aldehyde compounds by tandem dehydrogenation of dimethylamine-borane in the presence of a reduced graphene oxide furnished platinum nanocatalyst, *Catal. Sci. Technol.* 6 (2016) 2318–2324, <https://doi.org/10.1039/c5cy01462j>.
- [36] L. Shi, Y. Liu, Q. Liu, B. Wei, G. Zhang, Selective reduction of aldehydes and ketones to alcohols with ammonia borane in neat water, *Green Chem.* 14 (2012) 1372, <https://doi.org/10.1039/c2gc00006g>.
- [37] Y. Zhou, Z. Li, Y. Liu, J. Huo, C. Chen, Q. Li, S. Niu, S. Wang, Regulating hydrogenation chemoselectivity of α,β -unsaturated aldehydes by combination of transfer and catalytic hydrogenation, *ChemSusChem* 13 (2020) 1746–1750, <https://doi.org/10.1002/cssc.201902629>.
- [38] Q. Yang, Y.Z. Chen, Z.U. Wang, Q. Xu, H.L. Jiang, One-pot tandem catalysis over Pd@MIL-101: Boosting the efficiency of nitro compound hydrogenation by coupling with ammonia borane dehydrogenation, *Chem. Commun.* 51 (2015) 10419–10422, <https://doi.org/10.1039/c5cc03102h>.
- [39] Y.H. Zhou, Q. Yang, Y.Z. Chen, H.L. Jiang, Low-cost CuNi@MIL-101 as an excellent catalyst toward cascade reaction: Integration of ammonia borane dehydrogenation with nitroarene hydrogenation, *Chem. Commun.* 53 (2017) 12361–12364, <https://doi.org/10.1039/c7cc06530b>.
- [40] R. Dai, F. Peng, P. Ji, K. Lu, C. Wang, J. Sun, W. Lin, Electron crystallography reveals atomic structures of metal-organic nanolatexes with M₁₂(μ₃-O)₈(μ₃-OH)₈(μ₂-OH)₆ (M = Zr, Hf) secondary building units, *Inorg. Chem.* 56 (2017) 8128–8134, <https://doi.org/10.1021/acs.inorgchem.7b00845>.
- [41] B. An, J. Zhang, K. Cheng, P. Ji, C. Wang, W. Lin, Confinement of ultrasmall Cu/ZnO_x nanoparticles in metal-organic frameworks for selective methanol synthesis from catalytic hydrogenation of CO₂, *J. Am. Chem. Soc.* 139 (2017) 3834–3840, <https://doi.org/10.1021/jacs.7b00058>.
- [42] H. Wu, Y.S. Chua, V. Krungleviciute, M. Tyagi, P. Chen, T. Yildirim, W. Zhou, Unusual and highly tunable missing-linker defects in zirconium metal-organic framework UiO-66 and their important effects on gas adsorption, *J. Am. Chem. Soc.* 135 (2013) 10525–10532, <https://doi.org/10.1021/ja404514r>.
- [43] W.S. Hummers, R.E. Offeman, Preparation of graphitic oxide, *J. Am. Chem. Soc.* 80 (2002), <https://doi.org/10.1021/ja01539a017>.
- [44] H.X. Zhong, J. Wang, Y.W. Zhang, W.L. Xu, W. Xing, D. Xu, Y.F. Zhang, X.B. Zhang, ZIF-8 derived graphene-based nitrogen-doped porous carbon sheets as highly

- efficient and durable oxygen reduction electrocatalysts, *Angew. Chem. Int. Ed.* 53 (2014) 14235–14239, <https://doi.org/10.1002/anie.201408990>.
- [45] Z. Wei, R. Pan, Y. Hou, Y. Yang, Y. Liu, Graphene-supported Pd catalyst for highly selective hydrogenation of resorcinol to 1,3-cyclohexanedione through giant π -conjugate interactions, *Sci. Rep.* 5 (2015) 1–9, <https://doi.org/10.1038/srep15664>.
- [46] M. Zhao, Q. Lu, Q. Ma, H. Zhang, Two-dimensional metal-organic framework nanosheets, *Small Methods* 1 (2017), 1600030, <https://doi.org/10.1002/smt.201600030>.
- [47] L. Chen, H. Chen, Y. Li, One-pot synthesis of Pd@MOF composites without the addition of stabilizing agents, *Chem. Commun.* 50 (2014) 14752–14755, <https://doi.org/10.1039/c4cc06568a>.
- [48] D. Sun, Z. Li, Double-solvent method to Pd nanoclusters encapsulated inside the cavity of $\text{NH}_2\text{-UiO-66(Zr)}$ for efficient visible-light-promoted Suzuki coupling reaction, *J. Phys. Chem. C* 120 (2016) 19744–19750, <https://doi.org/10.1021/acs.jpcc.6b06710>.
- [49] H. Ye, H. Zhao, Y. Jiang, H. Liu, Z. Hou, Catalytic transfer hydrogenation of the C=O bond in unsaturated aldehydes over Pt nanoparticles embedded in porous UiO-66 nanoparticles, *ACS Appl. Nano Mater.* 3 (2020) 12260–12268, <https://doi.org/10.1021/acsanm.0c02735>.
- [50] K. Ralphs, É. McCourt, C. Ormandy, T.A. Carneiro de Souza, P. Nockemann, J. Jacquemin, H.G. Manyar, Highly selective reduction of α,β -unsaturated aldehydes and ketones under ambient conditions using tetraalkylphosphonium-based ionic liquids, *ChemistrySelect* 3 (2018) 11706–11711, <https://doi.org/10.1021/acsanm.0c02735>.
- [51] N. Luo, J. Liao, L. Ouyang, H. Wen, J. Liu, W. Tang, R. Luo, Highly pH-dependent chemoselective transfer hydrogenation of α,β -unsaturated aldehydes in water, *Organometallics* 38 (2019) 3025–3031, <https://doi.org/10.1021/acs.organomet.9b00353>.
- [52] Q. Han, Y. Liu, D. Wang, F. Yuan, X. Niu, Y. Zhu, Effect of carbon nanosheets with different graphitization degrees as a support of noble metals on selective hydrogenation of cinnamaldehyde, *RSC Adv.* 6 (2016) 98356–98364, <https://doi.org/10.1039/c6ra17979g>.
- [53] S. Wei, Y. Zhao, G. Fan, L. Yang, F. Li, Structure-dependent selective hydrogenation of cinnamaldehyde over high-surface-area $\text{CeO}_2\text{-ZrO}_2$ composites supported Pt nanoparticles, *Chem. Eng. J.* 322 (2017) 234–245, <https://doi.org/10.1016/j.cej.2017.04.026>.
- [54] S. Song, X. Liu, J. Li, J. Pan, F. Wang, Y. Xing, X. Wang, X. Liu, H. Zhang, Confining the nucleation of Pt to *in situ* form (Pt-Enriched Cage)@ CeO_2 Core@Shell nanostructure as excellent catalysts for hydrogenation reactions, *Adv. Mater.* 29 (2017), 1700495, <https://doi.org/10.1002/adma.201700495>.
- [55] Y. Zhang, S. Wei, Y. Lin, G. Fan, F. Li, Dispersing metallic platinum on green rust enables effective and selective hydrogenation of carbonyl group in cinnamaldehyde, *ACS Omega* 3 (2018) 12778–12787, <https://doi.org/10.1021/acsomega.8b02114>.
- [56] W. Xu, H. Fan, G. Wu, P. Chen, Comparative study on reducing aromatic aldehydes by using ammonia borane and lithium amidoborane as reducing reagents, *New J. Chem.* 36 (2012) 1496, <https://doi.org/10.1039/c2nj40227k>.
- [57] X. Yang, T. Fox, H. Berke, Ammonia borane as a metal free reductant for ketones and aldehydes: a mechanistic study, *Tetrahedron* 67 (2011) 7121–7127, <https://doi.org/10.1016/j.tet.2011.06.104>.
- [58] F. Delbecq, P. Sautet, Competitive $\text{C}\equiv\text{C}$ and C=O adsorption of α,β -unsaturated aldehydes on Pt and Pd surfaces in relation with the selectivity of hydrogenation reactions: a theoretical approach, *J. Catal.* 152 (1995) 217–236, <https://doi.org/10.1006/jcat.1995.1077>.
- [59] J. Huo, M. Marcello, A. Garai, D. Bradshaw, MOF-polymer composite microcapsules derived from pickering emulsions, *Adv. Mater.* 25 (2013) 2717–2722, <https://doi.org/10.1002/adma.201204913>.